J Mater Sci (2018) 53:12399–12406

Energy materials

In situ synthesis of chemically ordered primitive cubic Pt_3Co nanoparticles by a spray paint drying method for hydrogen evolution reaction

Zhenzhi Cheng[1], Xinpei Geng[1], Leyi Chen[1], Cheng Zhang[1], Haifu Huang[2], Shaolong Tang[1,*], and Youwei Du[1]

[1] *Collaborative Innovation Center of Advanced Microstructures, Jiangsu Key Laboratory for Nanotechnology, Nanjing National Laboratory of Microstructures and School of Physics, Nanjing University, Nanjing 210093, People's Republic of China*

[2] *Guangxi Key Laboratory for Relativistic Astrophysics, Guangxi Colleges and Universities Key Laboratory of Novel Energy Materials and Related Technology, Guangxi Novel Battery Materials Research Center of Engineering Technology, Guangxi Key Laboratory of Processing for Non-ferrous Metallic and Featured Materials, Guangxi University School of Physical Science and Technology, Guangxi University, Nanning 530004, People's Republic of China*

Received: 24 February 2018
Accepted: 24 May 2018
Published online: 31 May 2018

ABSTRACT

A facile two-step method is developed for large-scale synthesis of chemically ordered Pt_3Co nanoparticles (NPs) as a high-performance catalyst for hydrogen evolution reaction. Due to the NaCl-matrix as dispersing media avoids the severe aggregation during the high-temperature annealing process, the resulting Pt_3Co NPs are pure and well crystallized with narrow size distribution. Furthermore, the chemically ordered Pt_3Co NPs exhibit excellent HER property in acidic solution. Our methodology can be also applied to synthesis of other Pt-based NPs.

Introduction

With the shortage of fossil energy and more attention to environmental protection, hydrogen energy has attracted more and more interest for its zero emissions to the environment and high energy density [1, 2]. Due to the excellent corrosion resistance, high activity, stability and durability, noble metals are critical industry catalysts and used in many fields, such as catalytic conversion [3], hydrogen evolution reaction (HER) [4] and oxygen reduction reaction (ORR) [5]. During the past decades, electrocatalytic water splitting has been considered as a promising method to produce hydrogen owing to its clean process and high energy conversion efficiency [6]. However, the scarcity and high cost of noble metals impede its application and promotion. To overcome the issues of the noble metal catalysts, various approaches have been explored, such as reducing the noble metals loadings, increasing activity and enhancing durability. The demonstrated pathways to reduce the noble metals loadings and improve Pt utilization include decreasing the size of catalyst particles and constructing core–shell structures with

Address correspondence to E-mail: tangsl@nju.edu.cn

https://doi.org/10.1007/s10853-018-2497-8

an abundant metal core coated by a noble metal shell [7–9]. Regarding of achieving high activity and enhanced durability, considerable effects have been made on alloying Pt with 3d-transition metals [10–13] and exposing highly active lattice planes on their surface [14–16]. Studies show that Pt-M (Fe, Co, Ni, Cu) alloy with a chemically ordered structures performs the better activity and durability [17–19]. However, the prepared Pt_3Co alloy nanoparticles often have a chemically disordered face-centered cubic (fcc) lattice, whose activity and durability are lower than the chemically ordered structure. In order to obtain chemically ordered structures, high-temperature heat treatment is usually necessary, which is inevitably leading to the aggregation and growth of nanoparticles. Faced with this challenge, many methods have been put forward, such as encapsulating the nanoparticles with oxide like silicon dioxide or magnesium oxide [20–22], milling the FePt nanoparticles with sodium chloride to make the nanoparticles monodisperse in the NaCl-matrix [23, 24]. But all of these strategies need to fabricate the corresponding alloy nanoparticles firstly, which is complicated and highly demands for the process.

Here, we report an approach for large-scale production of chemically ordered Pt_3Co NPs with an average size of 7.14 nm via a spray paint drying method (SPD method) combined with a post-annealing treatment. In the synthesis, the NaCl-matrix serves as a reactor for alloying of the reduced metal and effectively prevents Pt_3Co NPs from coalescence during the annealing [25]. As a result, the chemically ordered Pt_3Co NPs exhibit a high mass current density of 667.9 A g^{-1} (Pt) at − 0.05 V, and only 3.3% loss after 5000 cycles while commercial Pt/C reduces by almost 28.5% for HER in 0.5 M H_2SO_4.

Experiments

Materials

Cobaltous nitrate ($Co(NO_3)_2{\cdot}6H_2O$)(99.99%), sodium chloride (NaCl) (99.99%) and hexadecane thiol (HDT)(97.0% GC) were purchased from Aladdin Reagent Co., Ltd. (Shanghai, China). Oleic acid (OA) and hexachloroplatinic acid ($H_2PtCl_6{\cdot}6H_2O$) were purchased from Sinopharm Chemical Reagent Co., Ltd. (Shanghai, China). Vulcan XC-72R carbon powder was purchased from Cabot Corporation (USA). Commercial Pt/C was purchased from Johnson Matthey.

Synthesis of Pt_3Co NPs

The Pt_3Co NPs were prepared using a SPD method. In a typical synthesis, 1 g of hexachloroplatinic acid ($H_2PtCl_6{\cdot}6H_2O$), 187.3 mg of cobaltous nitrate ($Co(NO_3)_2{\cdot}6H_2O$) and 11.87 g of sodium chloride (NaCl) were dissolved in 50 mL deionized water. After ultrasonic dissolving for 10 min, the mixed solution was sprayed on a quartz plate which was kept at 270 °C. As the solvent evaporated off instantly, a molecular level mixture of chemical composition (salt precursor) remained on the quartz plate. Then, the mixture was annealed at 500 and 700 °C under a H_2/Ar atmosphere for 2 h. The products are denoted as Pt_3Co-500 and Pt_3Co-700. Finally, the Pt_3Co NPs monodispersed in NaCl-matrix was obtained.

Preparation of Pt_3Co colloid

Hundred and fifty milligrams of salt-nanoparticle complex (containing 5 mg of Pt_3Co NPs) was scattered into a solution, which was composed of 30 mL hexane, 150 μL hexadecane thiol (HDT) and 150 μL oleic acid (OA). After being sonicated for 30 min, the NPs were transferred into the oil phase successfully and form a red colloid.

Preparation of carbon-supported Pt_3Co catalysts

Twenty milligrams of Vulcan XC-72R was added into the above-prepared colloid, and the mixture was sonicated for 60 min. Then, the mixture was dried and annealed at 500 °C for 2 h to remove the oil. That the carbon-supported Pt_3Co (C-Pt_3Co) was successfully prepared. Finally, the C-Pt_3Co catalyst was dispersed in a mixture of deionized water, isopropanol and Nafion (5%) (v/v/v 3:1:0.05) to form a 2 mg mL^{-1} catalyst ink. A glassy carbon electrode (5 mm diameter) was polished, and then 20 μL of catalyst ink was deposited on it and dried at ambient condition.

Electrochemical measurements

Electrochemical studies were conducted by a CHI 660D electrochemical workstation with a three-electrode cell at room temperature using a 0.5 M H_2SO_4

aqueous solution. A platinum wire was used as the counter electrode and Ag/AgCl (3 M KCl) as a reference electrode, which was calibrated with respect to a reversible hydrogen electrode (RHE). The HER polarization curves were recorded by linear sweep voltammetry with scan rate of 20 mV s^{-1}, while the scan rate for durability test was 50 mV s^{-1} between − 0.3 and 0.9 V potential.

Characterization of samples

The XRD patterns were recorded on an X-ray diffractometer (Rigaka Ultima IV multipurpose X-ray diffractometer) with a Cu-Kα radiation source over the range of 5–95° (scanning rate of 10° min^{-1}). X-ray photoelectron spectroscopy (XPS) studies were carried out on a Phi 5000 Versa Probe Scanning ESCA Microprobe (Ulvac-Phi, Inc., Japan), and all binding energies were referenced to the C 1*s* peak at 284.8 eV of the surface adventitious carbon to correct the shift caused by charge effect. The magnetic properties were measured using a Superconducting Quantum Interface Device (SQUID) (Quantum Design) with the magnetic field up to 60 kOe at the temperature of 2 K. Transmission electron microscopy (TEM) and high-resolution TEM (HRTEM) images were recorded on the JEM-2100HR JEOL (Japan) TEM, operating at 200 kV. The electrochemical performance measurements were taken using the electrochemical workstation (CHI 660D, Chenhua Instruments, China).

Results and discussion

The schematic illustration for the fabrication of Pt_3Co NPs is shown in Fig. 1. First, a mixed solution of specific proportion of sodium chloride, cobaltous chloride and chloroplatinic acid is prepared (Fig. 1a). Second, the solution was atomized and sprayed on a heated quartz plate (Fig. 1b). With the solvent evaporating instantly, each component precipitate simultaneously forms a uniformly mixed-salt precursor (Fig. 1c). Third, an annealing treatment is utilized to get Pt_3Co NPs (Fig. 1d). According to the phase diagram of Pt–Co alloy [26], the ordered primitive cubic phase is more stable than disordered phase (fcc) below 750 °C. But the prepared Pt_3Co alloy NPs often has a disordered phase. High-temperature treatment can promote the diffusion of atoms to realize an ordered arrangement [27]. In ordered to optimize the

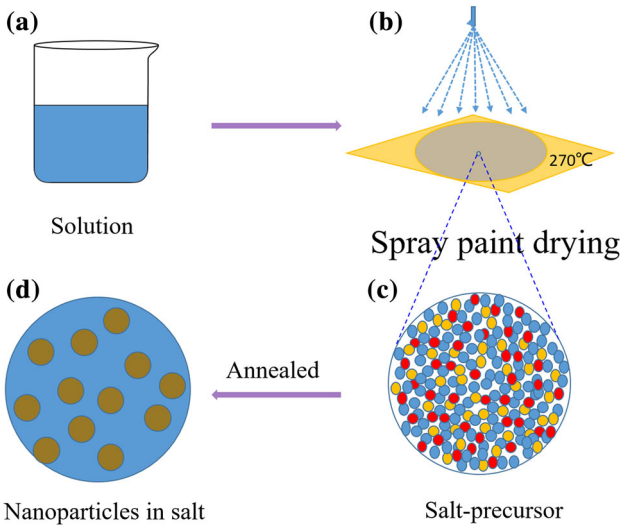

Figure 1 Schematic illustration for the synthesis of chemically ordered Pt_3Co NPs.

electrochemical performance of Pt_3Co NPs, the different phases of Pt_3Co NPs can be converted by controlling the annealing temperature.

Typical X-ray diffraction (XRD) patterns of the bulk structural information of as-synthesized Pt_3Co-500 and Pt_3Co-700 NPs are shown in Fig. 2a. As can be seen, seven well-defined diffraction peaks are observed at 2θ values of 40.5°, 47.1°, 68.8°, 83.0° and 87.6°. All of these peaks can be successfully indexed to (111), (200), (220), (311) and (222) plane reflections of the fcc-Pt_3Co. Compared with the fcc-Pt_3Co, there are two obvious additional diffraction peaks at 23.1° and 32.8° corresponding to (100) and (110) for Pt_3Co-700, suggesting that chemically ordered primitive cubic ($L1_2$) Pt_3Co NPs have been successful prepared after annealing at 700 °C for 2 h in Ar/H_2 atmosphere. The more detailed elemental composition of the as-prepared samples is further characterized by X-ray photoemission spectroscopy (XPS), as shown in Fig. 2c, d. The Pt 4f spectrum exhibits two contributions, 4 $f_{7/2}$ and 4 $f_{5/2}$ (resulting from the spin–orbit splitting), located at, respectively, 71.40 and 74.47 eV, upshifting of about 0.2 eV from the standard Pt 4 $f_{7/2}$ and Pt 4 $f_{5/2}$ peaks at 71.20 and 74.53 eV, indicating that the Pt_3Co alloy is successfully prepared [28–31]. For the Co 2 $p_{3/2}$, there is a peak at 780.6 eV, indicating that the surface of the NPs is slightly oxidized when the NPs is exposed to the air. Furthermore, the calculated atomic ratio of Pt to Co is approximatively 3 for Pt_3Co-500, while 4.67 for Pt_3Co-700. As XPS is a surface analysis technique, there probably is a Pt-rich

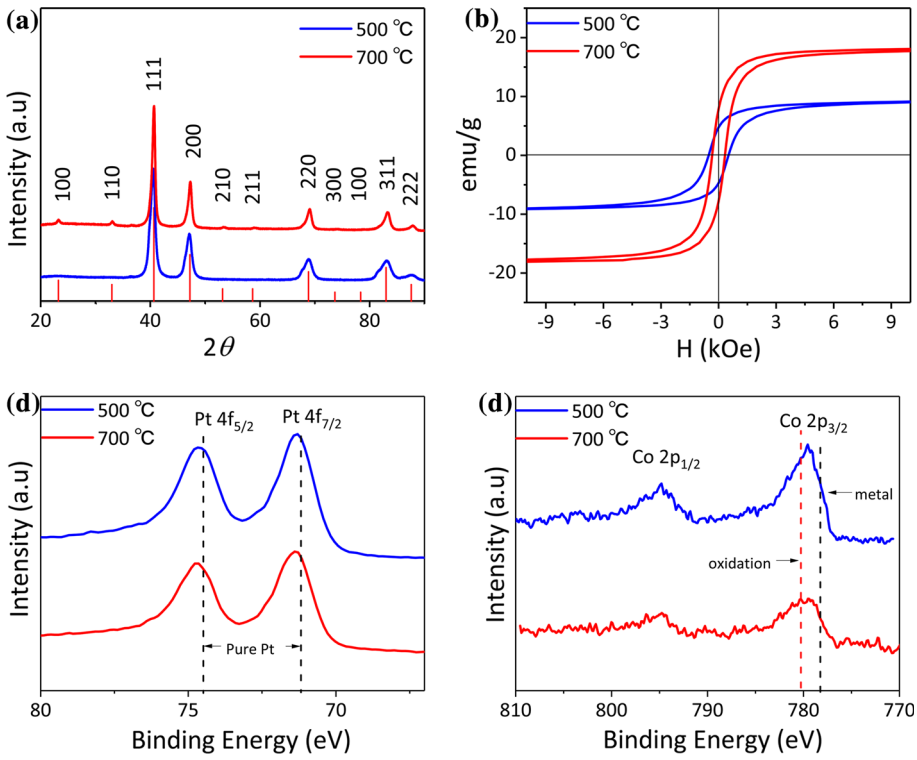

Figure 2 **a** XRD patterns of Pt_3Co-500 and Pt_3Co-700. **b** Hysteresis loops of Pt_3Co-500 and Pt_3Co-700 measured at 2 K. **c** The Pt 4f high-resolution XPS spectra for Pt_3Co-500 and Pt_3Co-700. **d** The Co 2p high-resolution XPS spectra for Pt_3Co-500 and Pt_3Co-700.

shell encasing the Pt_3Co-700 NPs [17, 22, 32]. All the results from XRD and XPS suggest that pure and well crystallized chemically ordered Pt_3Co NPs have been obtained by our simply method. In addition, Fig. 2b shows the hysteresis loop of Pt_3Co nanocrystals annealed at different temperatures. It can be found that the saturation magnetization increases with the increasing annealing temperature. It can be attributed to the size growing of the NPs resulting from the higher temperature, which is consistent with previous reports [33, 34].

The morphology and structure of the as-prepared samples are investigated by transmission electron microscopy (TEM). Figure 3a–d shows low- and high-magnification TEM images of the Pt_3Co-500 and Pt_3Co-700 NPs. The low-magnification images (Fig. 3a, c) indicate that the NPs exhibit a narrow size distribution and well crystallized. Moreover, it can be observed that the Pt_3Co-500 NPs show a spherical morphology, while the Pt_3Co-700 NPs exhibit polygon morphology under a higher annealing temperature. Clearly, the magnified images (Fig. 3b, d) show that there is one lattice spacing, about 0.22 nm, which corresponds to (111) lattice planes of Pt_3Co NPs. Figure 3e shows the size distribution of Pt_3Co-500 and Pt_3Co-700. It can be seen, the as-synthesized Pt_3Co-500 NPs have an average size 5.8 nm with a narrow size distribution, and the Pt_3Co-700 is about 7.1 nm. As shown in Fig. 3f, the Pt_3Co NPs are monodispersed in the NaCl-matrix with a uniform size during the annealing process, which plays a key factor in inhibiting the growth of the NPs. As a result, the NPs just show slightly growth in size even annealed at 700 °C. It should emphasize that the controlled size is an important way in realizing high utilization of Pt. After transferred into hexane, the Pt_3Co NPs are well dispersed forming a red colloid (Fig. 3g), which further confirms that our samples have a small and uniform size.

To explore the structure effect on the catalytic performance, the synthesized Pt_3Co-500 and Pt_3Co-700 NPs are incorporated into carbon black and applied as electrocatalysts for the HER. The HER performance of as-synthesized Pt_3Co NPs and the contrastive commercial Pt/C are measured in 0.5 M H_2SO_4 solution by a three-electrode system with a platinum sheet counter electrode. The normalized HER polarization curves of different catalysts are displayed in Fig. 4. As expected, the Pt_3Co-700 NPs own the best electrocatalytic activity. Pt_3Co-700 NPs exhibit a small onset potential in Fig. 4a. The overpotential is only − 32.6 and − 34.0 mV on the Pt_3Co-700 NPs and Pt_3Co-500 NPs, respectively, 3 mV and 1.6 mV lower than that on commercial Pt/C at a

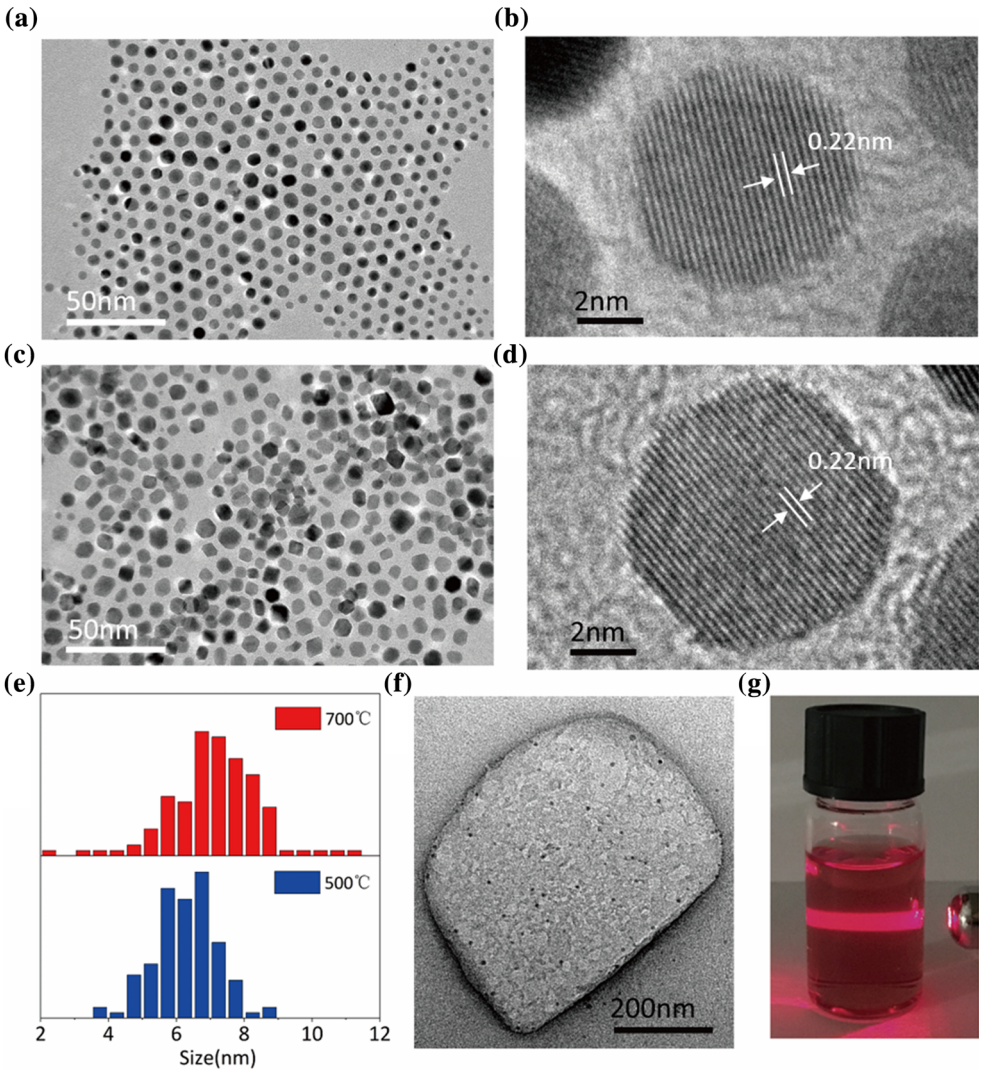

Figure 3 **a**–**b** Low- and high-magnification TEM images of Pt_3Co-500 NPs annealed at 500 °C. **c**–**d** Low- and high-magnification TEM images of Pt_3Co-700 NPs annealed at 700 °C. **e** The size distribution pattern of Pt_3Co-500 and Pt_3Co-700. **f** Pt_3Co NPs scattered in annealed NaCl-matrix. **g** Optical image of Pt_3Co-700 NPs dispersed in hexane.

current density of 10 mA cm^{-2}. Furthermore, the HER activities at the potential of − 0.05 V for the Pt_3Co-700 NPs, Pt_3Co-500 NPs and commercial Pt/C are 24.8, 21.1 and 19.3 mA/cm^2, respectively. As shown in Fig. 4b, the Tafel slope of the Pt_3Co-700 NPs is 28.6 mV $decade^{-1}$, even lower than that of commercial Pt/C 35.2 mV $decade^{-1}$, suggesting the HER rate of the Pt_3Co-700 NPs acquires a more rapid increase with overpotential decreasing. These reflect the best HER activity of the Pt_3Co-700 NPs. It is worth mentioning that the mass current density of the Pt_3Co-700 NPs could be much higher than commercial Pt/C (473.8 A g^{-1}) and fcc-Pt_3Co NPs (569.5 A g^{-1}, up to (667.9 A g^{-1}) (Pt) at − 0.05 V (Fig. 4d).

To further evaluate the application potential of the as-synthesized NPs as high-performance catalysts for HER, the durability of the Pt_3Co-700 NPs were executed by voltammetry (CV) sweeps between − 0.3 and 0.6 V for 5000 cycles. Clearly, the Pt_3Co-700 NPs do not show any obvious activity attenuation, as low as 1.5 mV after 5000 CV cycles at a current density of 10 mA cm^{-2}. However, the commercial Pt/C shows approximately 9 mV negative shift, as shown in Fig. 4c. A more significant difference in the stability is shown in Fig. 4d, and the Pt_3Co-700 NPs suffers from only 3.3% loss of the initial current density after 5000 cycles while commercial Pt/C reduces by almost 28.5% at − 0.05 V. The Pt_3Co-700 NPs perform enhanced HER activity and durability, due to the surface segregation effect which results in a Pt-rich shell on the surface of Pt_3Co-700 NPs. Furthermore, the chemically ordered structure exposes ideal catalytic lattice planes on their surface (Fig. 3c, d) and suppresses the cobalt etching in the acid [18]. Besides,

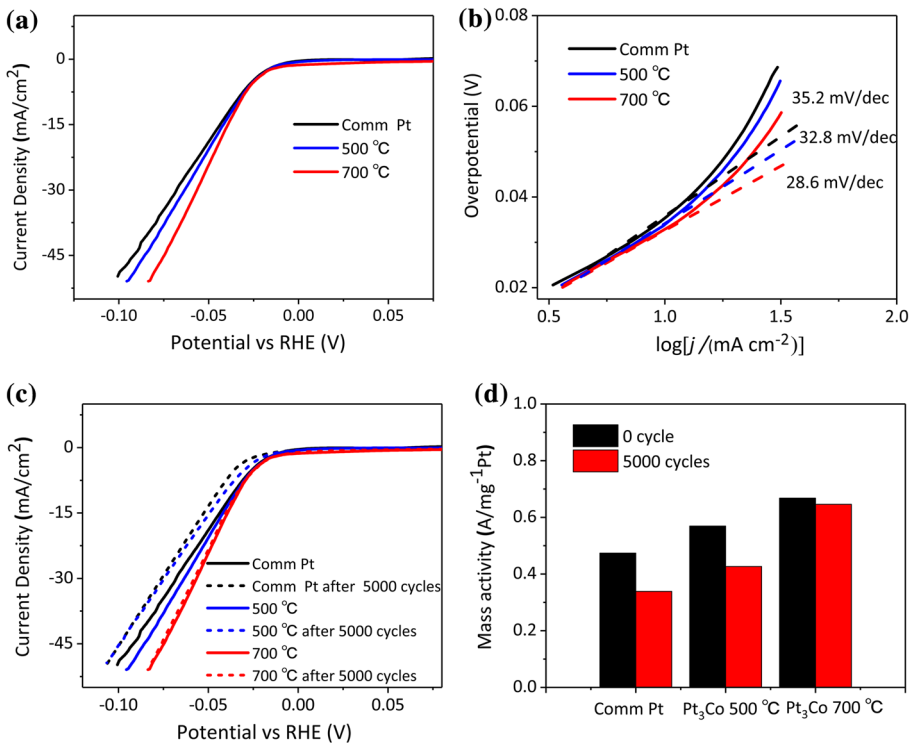

Figure 4 **a** The HER polarization curves of the commercial Pt/C, Pt_3Co-500 NPs and Pt_3Co-700 NPs normalized by electrode area, acquired by linear sweep voltammetry with a scan rate of 20 mV s^{-1} in 0.5 M H_2SO_4 solution at room temperature. **b** Durability test of the commercial Pt/C, Pt_3Co-500 NPs and Pt_3Co-700 NPs. **c** Corresponding Tafel plots obtained from polarization curves of above catalysts. **d** HER mass activity normalized by mass of Pt at − 0.05 V.

previous modeling studies show that, within the chemically ordered $L1_2$-Pt_3Co structure, synergy arising from the electronic spin–orbit coupling between Co and Pt makes the $L1_2$-Pt_3Co chemically much more active and stable [35–37].

Conclusion

In summary, we present a new SPD method combined with a post-annealing treatment to realize the monodispersing of the chemically ordered Pt_3Co NPs. In the synthesis, NaCl-matrix serves as a reactor for alloying of the reduced metal and prevents the NPs from sintering in high annealing temperature. Benefiting from the rational structural features, the chemically ordered Pt_3Co NPs show outstanding HER catalytic activity and excellent chemical stability against Co etching in the acid solution compared with chemically disordered Pt_3Co NPs. Such simply and conveniently synthetic strategy by NaCl-matrix packaging the as-grown precursor NPs during the annealing process is not limited to fabricate Pt_3Co NPs, but also provide a versatile approach to high-heat treatment needed NPs for important energy conversion applications.

Acknowledgements

The authors acknowledge financial support by the National Key Project of Fundamental Research of China (Grant No. 2012CB932304) and the National Natural Science Foundation of China (Grant Nos. 21203037 and 11264005).

Compliance with ethical standards

Conflict of interest The authors declared that they have no conflict of interest.

References

[1] Mallouk TE (2013) Water electrolysis: divide and conquer. Nat Chem 5:362–363

[2] Norskov JK, Christensen CH (2006) Toward efficient hydrogen production at surfaces. Science 312(5778):1322–1323

[3] Joo SH, Park JY, Tsung C-K, Yamada Y, Yang P, Somorjai GA (2009) Thermally stable Pt/mesoporous silica core–shell nanocatalysts for high-temperature reactions. Nat Mater 8:126–131

[4] Yin HJ, Zhao SL, Zhao K, Muqsit A, Tang HJ, Chang L, Zhao HJ, Gao Y, Tang ZY (2015) Ultrathin platinum

nanowires grown on single-layered nickel hydroxide with high hydrogen evolution activity. Nat Commun 6:6430

[5] Li M, Zhao Z, Cheng T, Fortunelli A, Chen C-Y, Yu R, Zhang Q, Gu L, Merinov B, Lin Z, Zhu E, Yu T, Jia Q, Guo J, Zhang L, Goddard WA III, Huang Y, Duan X (2016) Ultrafine jagged platinum nanowires enable ultrahigh mass activity for the oxygen reduction reaction. Science 354(6318):1414–1419

[6] Xie J, Xie Y (2015) Structural engineering of electrocatalysts for the hydrogen evolution reaction: Order or disorder? ChemCatChem 7(17):2568–2580

[7] Zhang L, Roling LT, Wang X, Vara M, Chi M, Liu J, Choi SI, Park J, Herron JA, Xie Z, Mavrikakis M, Xia Y (2015) Platinum-based nanocages with subnanometer-thick walls and well-defined, controllable facets. Science 349(6246):412–416

[8] Zhou M, Wang H, Vara M, Hood ZD, Luo M, Yang T-H, Bao S, Chi M, Xiao P, Zhang Y, Xia Y (2016) Quantitative analysis of the reduction kinetics responsible for the one-pot synthesis of Pd–Pt bimetallic nanocrystals with different structures. J Am Chem Soc 138(37):12263–12270

[9] Wang C, van der Vliet D, More KL, Zaluzec NJ, Peng S, Sun S, Daimon H, Wang G, Greeley J, Pearson J, Paulikas AP, Karapetrov G, Strmcnik D, Markovic NM, Stamenkovic VR (2011) Multimetallic Au/$FePt_3$ nanoparticles as highly durable electrocatalyst. Nano Lett 11(3):919–926

[10] Stamenkovic VR, Mun BS, Mayrhofer KJJ, Ross PN, Markovic NM (2006) Effect of surface composition on electronic structure, stability, and electrocatalytic properties of Pt-transition metal alloys: Pt-skin versus Pt-skeleton surfaces. J Am Chem Soc 128(27):8813–8819

[11] Lu S, Eid K, Ge D, Guo J, Wang L, Wang H, Gu H (2017) One-pot synthesis of PtRu nanodendrites as efficient catalysts for methanol oxidation reaction. Nanoscale 9:1033–1039

[12] Zhang H, Jin M, Xia Y (2012) Enhancing the catalytic and electrocatalytic properties of Pt-based catalysts by forming bimetallic nanocrystals with Pd. Chem Soc Rev 41:8035–8049

[13] Liu T, Wang K, Yuan Q, Shen Z, Wang Y, Zhang Q, Wang X (2017) Monodispersed sub-5.0 nm PtCu nanoalloys as enhanced bifunctional electrocatalysts for oxygen reduction reaction and ethanol oxidation reaction. Nanoscale 9:2963–2968

[14] Lim B, Jiang M, Camargo PHC, Cho EC, Tao J, Lu X, Zhu Y, Xia Y (2009) Pd–Pt bimetallic nanodendrites with high activity for oxygen reduction. Science 324(5932):1302–1305

[15] Tian N, Zhou Z-Y, Sun S-G, Ding Y, Wang ZL (2007) Synthesis of tetrahexahedral platinum nanocrystals with high-index facets and high electro-oxidation activity. Science 316(5825):732–735

[16] Wu J, Zhang J, Peng Z, Yang S, Wagner FT, Yang H (2010) Truncated octahedral Pt_3Ni oxygen reduction reaction electrocatalysts. J Am Chem Soc 132(14):4984–4985

[17] Wang DL, Xin HL, Hovden R, Wang HS, Yu YC, Muller DA, DiSalvo FJ, Abruna HD (2013) Structurally ordered intermetallic platinum–cobalt core–shell nanoparticles with enhanced activity and stability as oxygen reduction electrocatalysts. Nat Mater 12:81–87

[18] Kim J, Lee Y, Sun S (2010) Structurally ordered FePt nanoparticles and their enhanced catalysis for oxygen reduction reaction. J Am Chem Soc 132(14):4996–4997

[19] Wang D, Yu Y, Xin HL, Hovden R, Ercius P, Mundy JA, Chen H, Richard JH, Muller DA, DiSalvo FJ, Abruna HD (2012) Tuning oxygen reduction reaction activity via controllable dealloying: a model study of ordered Cu_3Pt/C intermetallic nanocatalysts. Nano Lett 12(10):5230–5238

[20] Hunt ST, Milina M, Alba-Rubio AC, Hendon CH, Dumesic JA, Román-Leshkov Y (2016) Self-assembly of noble metal monolayers on transition metal carbide nanoparticle catalysts. Science 352(6288):974–978

[21] Wong A, Liu Q, Griffin S, Nicholls A, Regalbuto J (2017) Synthesis of ultrasmall, homogeneously alloyed, bimetallic nanoparticles on silica supports. Science 358(6369):1427–1430

[22] Li Q, Wu L, Wu G, Su D, Lv H, Zhang S, Zhu W, Casimir A, Zhu H, Mendoza-Garcia A, Sun S (2015) New approach to fully ordered fct-FePt nanoparticles for much enhanced electrocatalysis in acid. Nano Lett 15(4):2468–2473

[23] C-B R, Li D, Nandwana V, Poudyal N, Ding Y, Wang ZL, Zeng H, Liu JP (2016) Size-dependent chemical and magnetic ordering in $L1_0$-FePt nanoparticles. Adv Mater 18(22):2984–2988

[24] Li Q, Sun SH (2016) Recent advances in the organic solution phase synthesis of metal nanoparticles and their electrocatalysis for energy conversion reactions. Nano Energy 29:178–197

[25] Ding W, Li L, Xiong K, Wang Y, Li W, Nie Y, Chen S, Qi X, Wei Z (2015) Shape fixing via salt recrystallization: a morphology-controlled approach to convert nanostructured polymer to carbon nanomaterial as a highly active catalyst for oxygen reduction reaction. J Am Chem Soc 137(16):5414–5420

[26] Hansen M, Anderko K (1958) Constitution of binary alloys, 2nd edn. McGraw-Hill, New York

[27] Berg H, Cohen JB (1972) Long-range order and ordering kinetics in $CoPt_3$. Metall Trans 3(7):1797–1805

[28] Xia T, Liu J, Wang S, Wang C, Sun Y, Wang R (2017) Nanomagnetic CoPt truncated octahedrons: facile synthesis, superior electrocatalytic activity and stability for methanol

oxidation. J Mater Sci 60(1):57–67. https://doi.org/10.1007/s40843-016-5139-y

[29] Zou L, Li J, Yuan T, Zhou Y, Li X, Yang H (2014) Structural transformation of carbon-supported Pt_3Cr nanoparticles from a disordered to an ordered phase as a durable oxygen reduction electrocatalyst. Nanoscale 6(18):10686–10692

[30] Wakisaka M, Mitsui S, Hirose Y, Kawashima K, Uchida H, Watanabe M (2006) Electronic structures of Pt–Co and Pt–Ru alloys for CO-tolerant anode catalysts in polymer electrolyte fuel cells studied by EC–XPS. J Phys Chem B 110(46):23489–23496

[31] Lu Y, Thia L, Fisher A, C-y J, Yi SC, Wang X (2017) Octahedral PtNi nanoparticles with controlled surface structure and composition for oxygen reduction reaction. J Mater Sci 60(11):1109–1120. https://doi.org/10.1007/s40843-017-9029-5

[32] Vasylyev MA, Tinkov VA, Blaschuk AG, Luyten J, Creemers C (2006) Thermo-stimulated surface segregation in the ordering alloy $Pt_{80}Co_{20}$ (1 1 1): experiment and modeling. Appl Surf Sci 253:1081–1089

[33] Murray C, Sun S, Doyle H, Betley T (2001) Monodisperse 3d transition-metal (Co, Ni, Fe) nanoparticles and their assembly into nanoparticle superlattices. MRS Bull 26(12):985–991

[34] Shevchenko EV, Talapin DV, Schnablegger H, Kornowski A, Festin Ö, Svedlindh P, Haase M, Weller H (2003) Study of nucleation and growth in the organometallic synthesis of magnetic alloy nanocrystals: the role of nucleation rate in size control of $CoPt_3$ nanocrystals. J Am Chem Soc 125(30):9090–9101

[35] Stamenković V, Schmidt TJ, Ross PN, Marković NM (2003) Surface segregation effects in electrocatalysis: kinetics of oxygen reduction reaction on polycrystalline Pt_3Ni alloy surfaces. J Electroanal Chem 554:191–199

[36] Stamenkovic VR, Mun BS, Arenz M, Mayrhofer KJ, Lucas CA, Wang G, Ross PN, Markovic NM (2007) Trends in electrocatalysis on extended and nanoscale Pt-bimetallic alloy surfaces. Nat Mater 6:241–247

[37] Šipr O, Minár J, Mankovsky S, Ebert H (2008) Influence of composition, many-body effects, spin-orbit coupling, and disorder on magnetism of Co–Pt solid-state systems. Phys Rev B 78:144403